supporting information

H-spilled storage to maximize the catalytic performances of Pd-based bimetals@$Ti_3C_2T_x$ MXene in selective semihydrogenations

Jing Zhao,[a],1 Yanzhuo Zhang,[b],1Hucheng Zhang,*[a] Haiyan Wang,[a] and Jianji Wang*[a]

[a]Collaborative Innovation Centre of Henan Province for Green Manufacturing of Fine Chemicals, Key Laboratory of Green Chemical Media and Reactions, Ministry of Education, School of Chemistry and Chemical Engineering, Henan Normal University, Xinxiang, Henan 453007, China. *E-mail: hzhang@htu.edu.cn; jwang@htu.edu.cn.

[b]School of Environment, Henan Normal University, Key Laboratory for Yellow River and Huai River Water Environmental and Pollution Control, Ministry of Education, Henan Key Laboratory for Environmental Pollution Control, International Joint Laboratory on Key Techniques in Water Treatment, Xinxiang, Henan 453007, P. R. China.

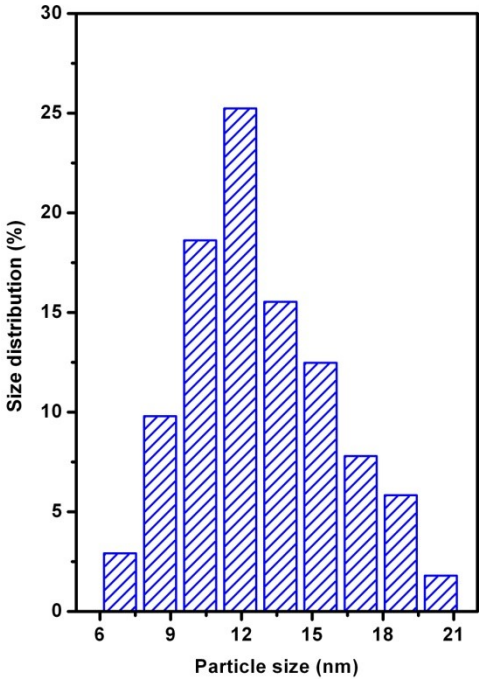

Fig S1. Size distribution of Pd-Ni alloy nanoparticles on $Pd_{1.8}Ni@Ti_3C_2T_x$.

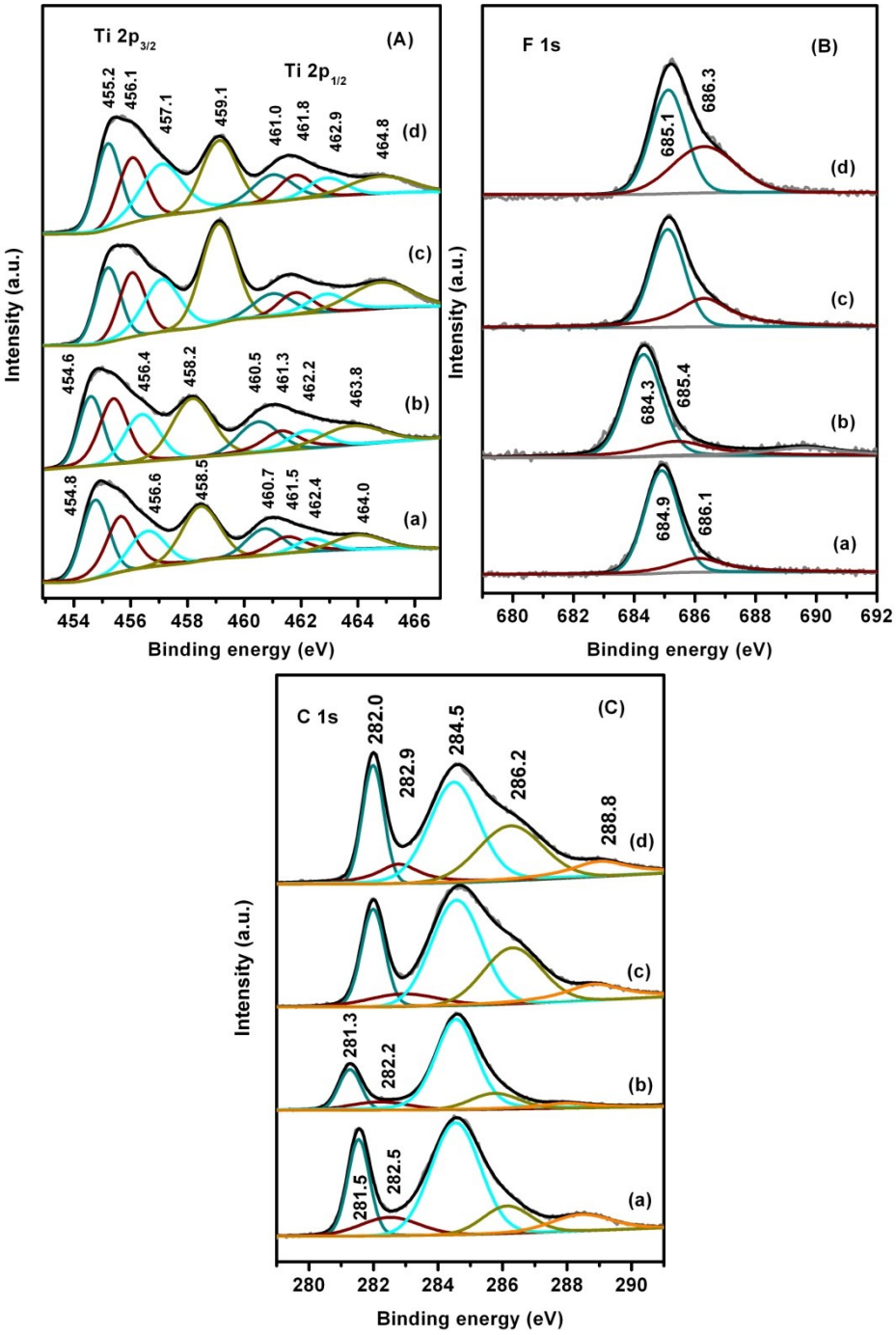

Fig S2. High-resolution XPS spectra of Ti 2p (A), F 1s (B), and C 1s (C) in $Pd@Ti_3C_2T_x$ (a), $Pd_{1.8}Ni@Ti_3C_2T_x$ (b), $Pd^H@Ti_3C_2T_x$ (c), and $Pd^H{}_{1.8}Ni@Ti_3C_2T_x$ (d). The XPS peaks of Ti $2p_{3/2}$ at 454.8, 455.7, 456.6, 458.5 eV in $Pd@Ti_3C_2T_x$ or 454.6, 454.4, 456.4, 458.2 eV in $Pd_{1.8}Ni@Ti_3C_2T_x$ are respectively assigned to Ti-C, Ti^{2+}, Ti^{3+}, and $TiO_{2-x}F_x$. The XPS peaks of F 1s at 684.9 and 685.1 eV in $Pd@Ti_3C_2T_x$ or 684.3 and 685.4 eV are respectively assigned to Ti-F and $TiO_{2-x}F_x$.

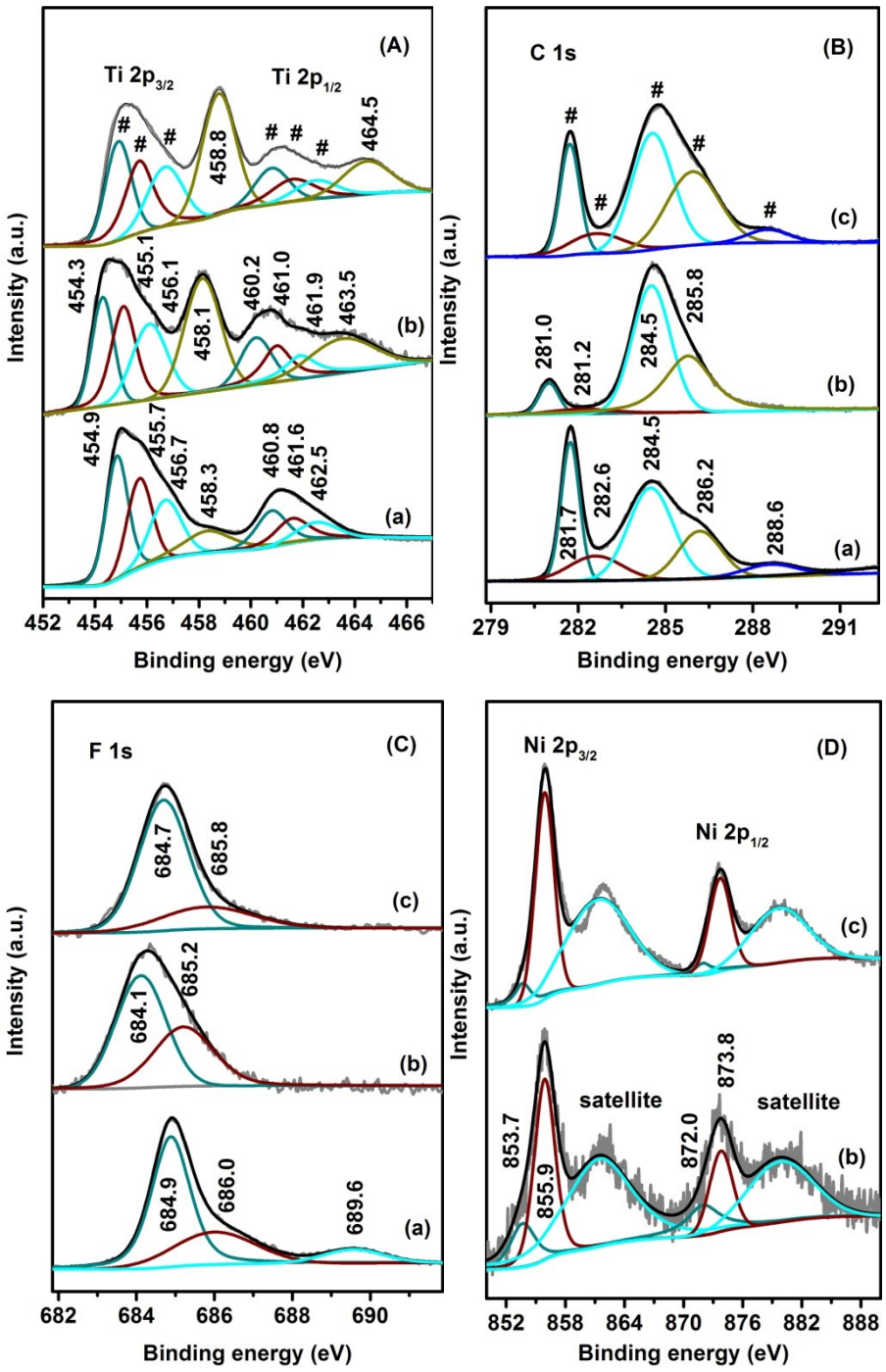

Fig S3. High-resolution XPS spectra of Ni 2p (A), Ti 2p (B), C 1s (C), and F 1s (D) in $Ti_3C_2T_x$ (a), $Pd_{1.9}Ni$@APTES-$Ti_3C_2T_x$ (b), and $Pd^H_{1.9}Ni$@APTES-$Ti_3C_2T_x$ (c). # denotes the same peak locus as that in $Ti_3C_2T_x$.

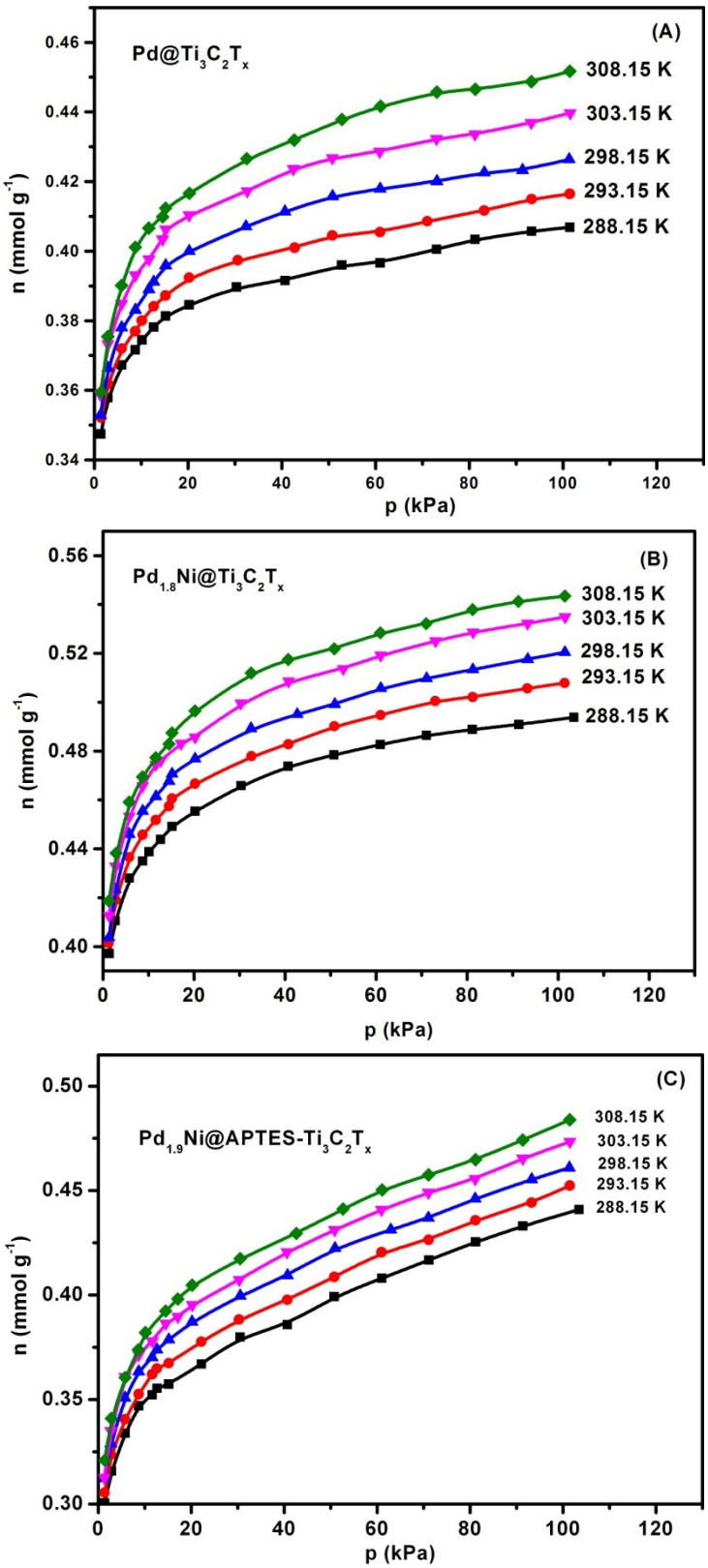

Fig S4. Isotherms of H_2 adsorption on $Pd@Ti_3C_2T_x$ (A), $Pd_{1.8}Ni@Ti_3C_2T_x$ (B), and $Pd_{1.9}Ni@APTES\text{-}Ti_3C_2T_x$ (C) with the temperature range from 288.15 to 308.15K.

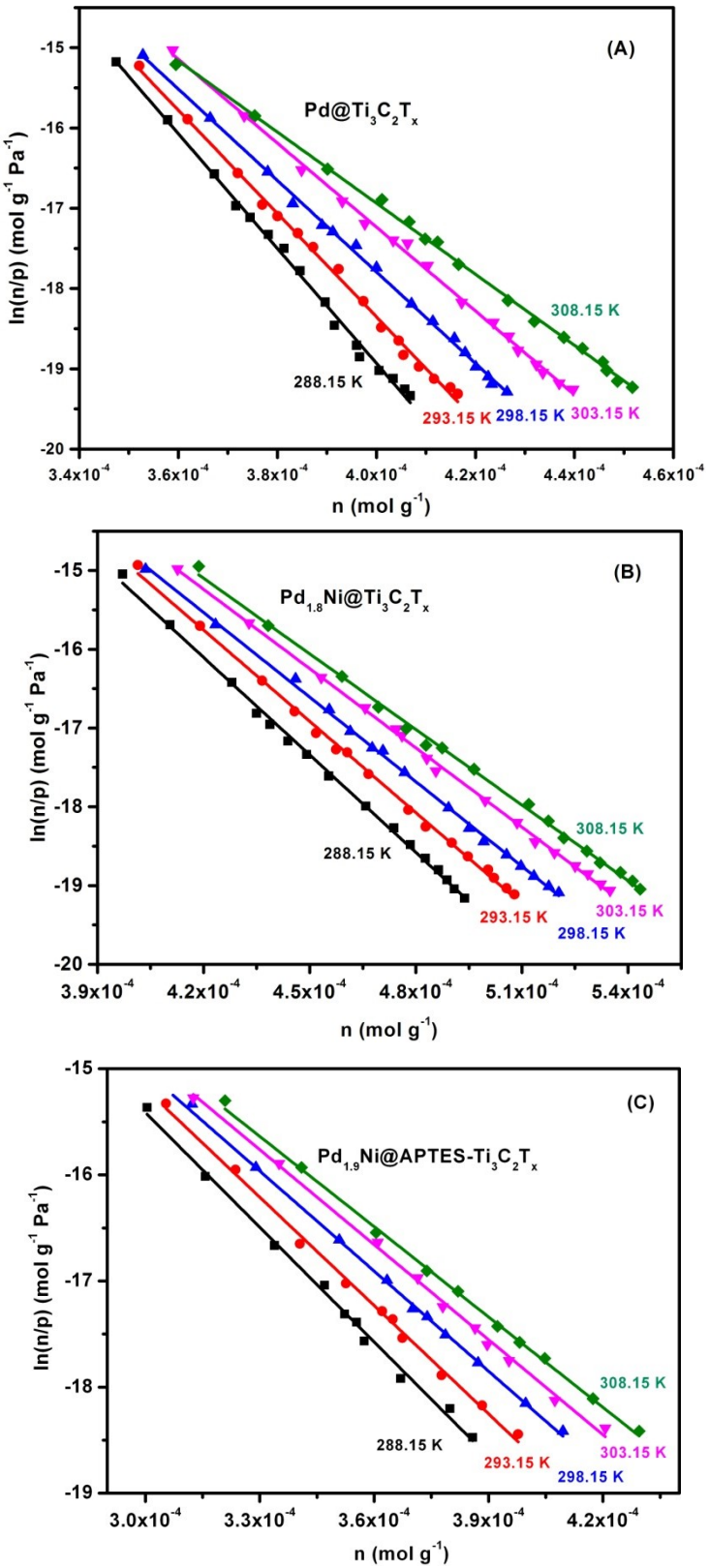

Fig S5. Virial graphs of H_2 adsorption on $Pd@Ti_3C_2T_x$ (A), $Pd_{1.8}Ni@Ti_3C_2T_x$ (B), and $Pd_{1.9}Ni@APTES\text{-}Ti_3C_2T_x$ (C) at different temperature. The lines were respectively fitted by the virial equation: $\ln(n/p) = A_0 + A_1n + A_2n^2 + \cdots$. Henry's law: $n = K0p$, K0 is Henry's law constant, $\ln K_0 = A_0$.

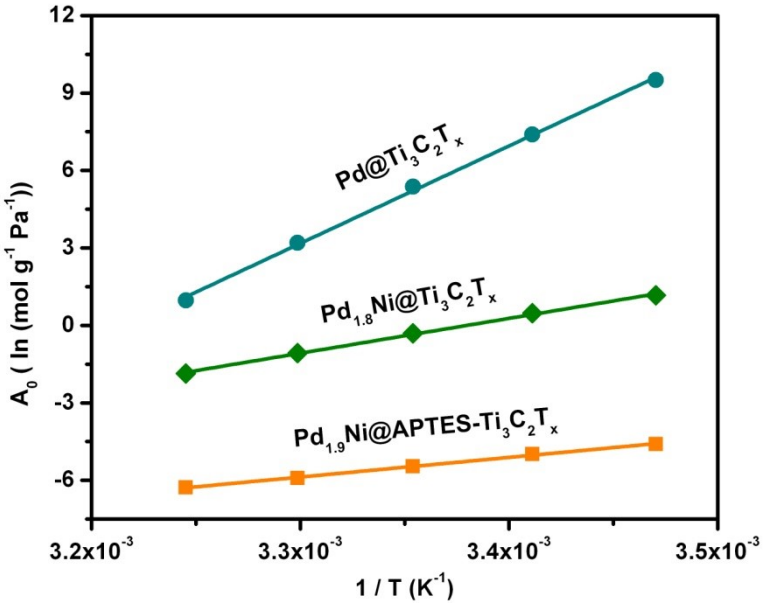

Fig S6. A_0 vs. 1/T for H_2 adsorption on $Pd@Ti_3C_2T_x$ (A), $Pd_{1.8}Ni@Ti_3C_2T_x$ (B), and $Pd_{1.9}Ni@APTES\text{-}Ti_3C_2T_x$ (C).

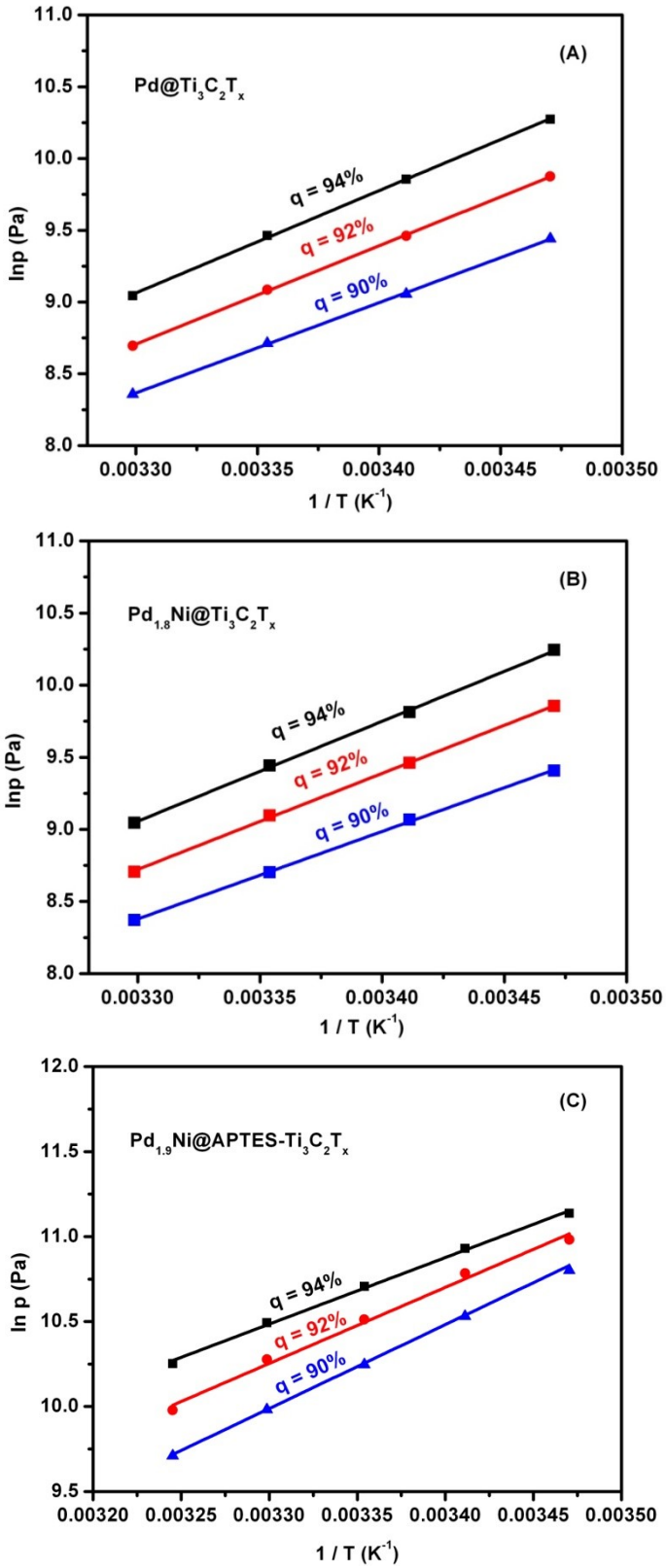

Fig. S7. Van't Hoff graphs of H_2 adsorption on $Pd@Ti_3C_2T_x$ (A), $Pd_{1.8}Ni@Ti_3C_2T_x$ (B), and $Pd_{1.9}Ni@APTES\text{-}Ti_3C_2T_x$ (C) with different q at 288.15K. Van't Hoff equation: $\ln p = -\Delta H_{ad} / RT + \cdots$

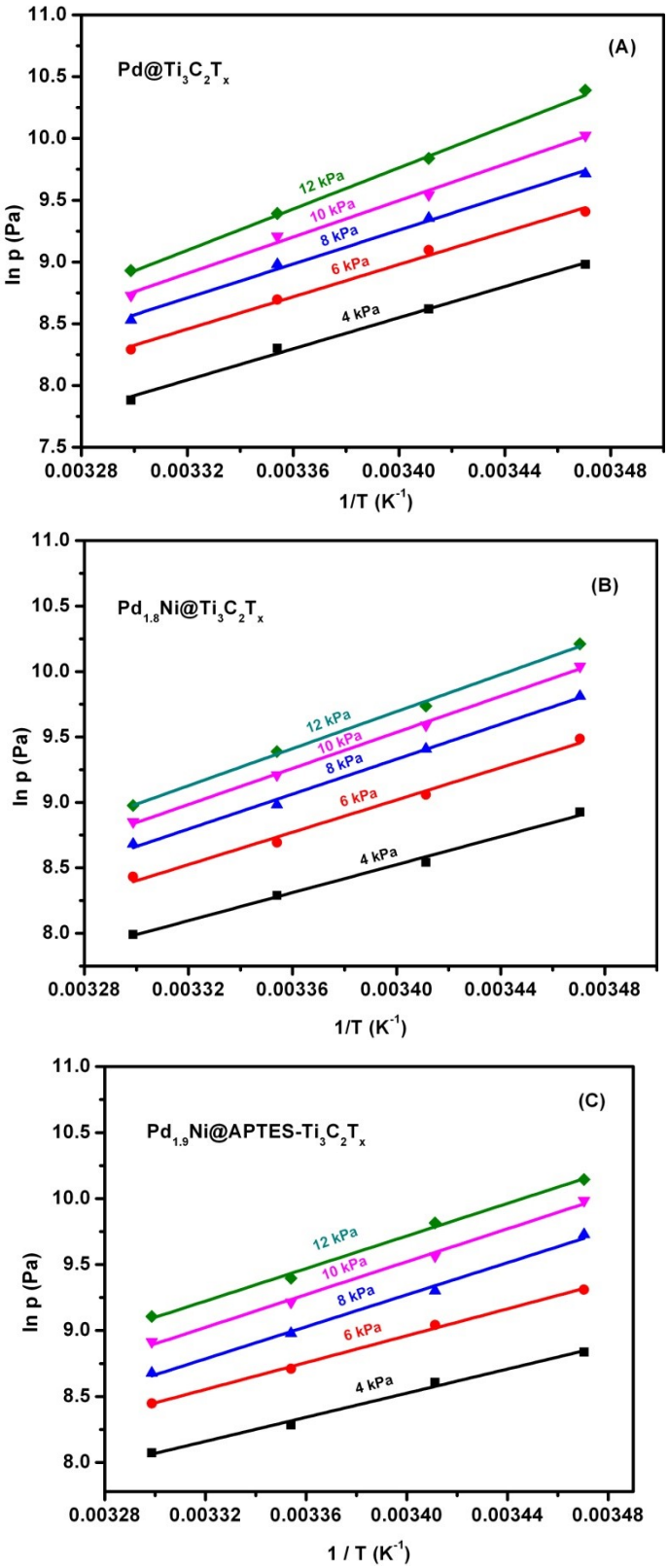

Fig S8. Van't Hoff graphs of H_2 adsorption on $Pd@Ti_3C_2T_x$ (A), $Pd_{1.8}Ni@Ti_3C_2T_x$ (B), and $Pd_{1.9}Ni@APTES\text{-}Ti_3C_2T_x$ (C) with the given pressures at 298.15K.

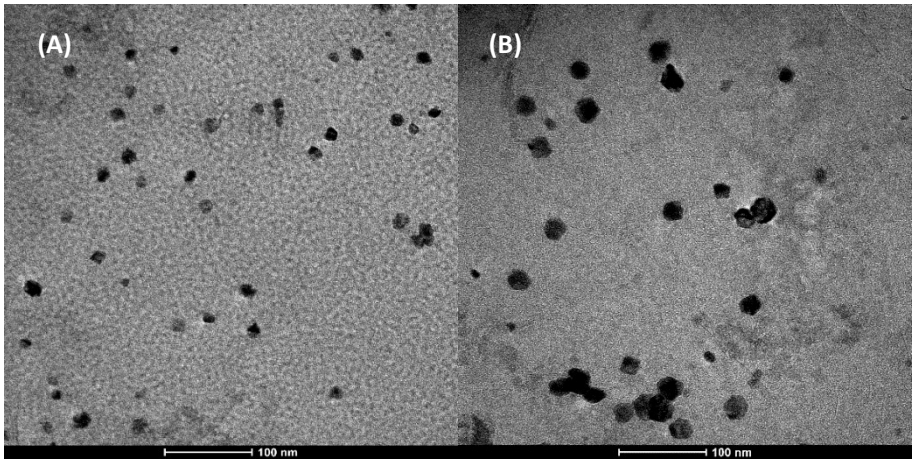

Fig S9. TEM images of $Pd_{2.6}Co@Ti_3C_2T_x$ (A) and $Pd_{1.5}Fe@Ti_3C_2T_x$ (B).

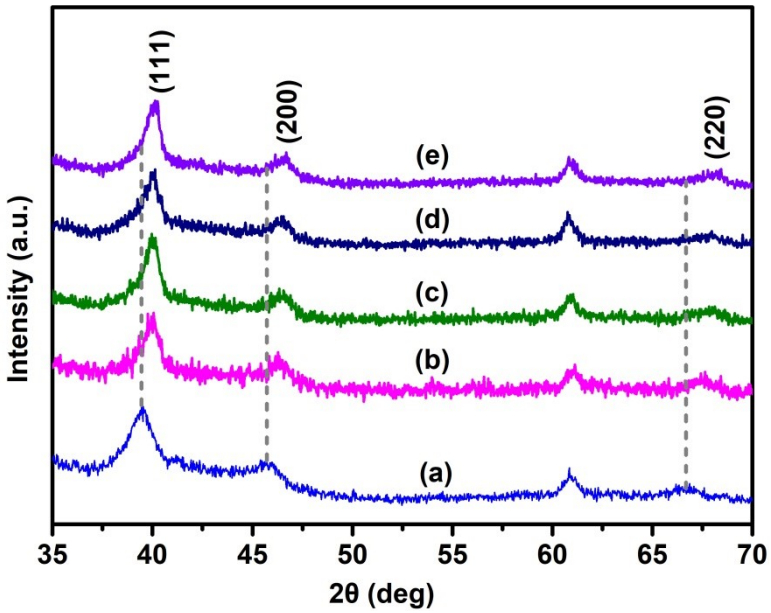

Fig S10. XRD patterns of $Pd@Ti_3C_2T_x$ (a), $Pd_{2.6}Co@Ti_3C_2T_x$ (b), $Pd_{2.8}Co@APTES\text{-}Ti_3C_2T_x$ (c), $Pd_{1.5}Fe@Ti_3C_2T_x$ (d), and $Pd_{1.7}Fe@APTES\text{-}Ti_3C_2T_x$ (e).

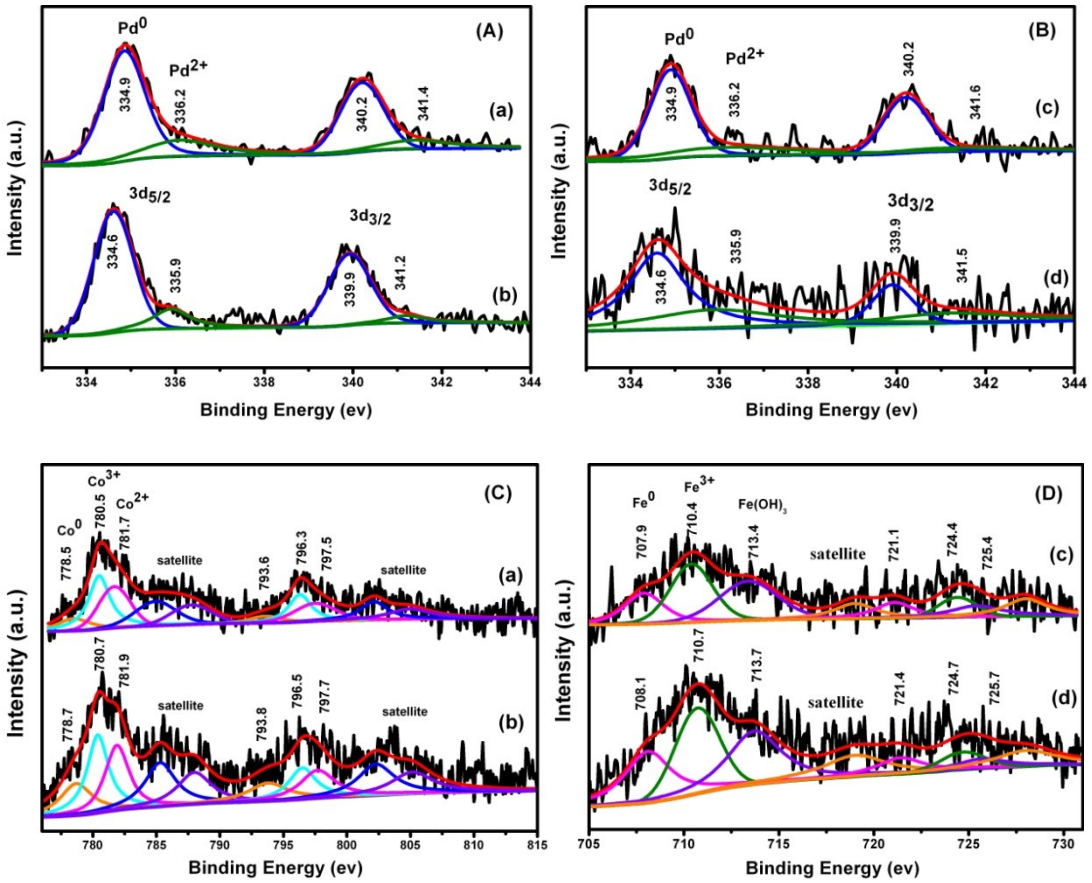

Fig S11. high-resolution XPS spectra of Pd 3d (A and B), Co 2p, and Fe 2p in $Pd_{2.6}Co@Ti_3C_2T_x$ (a), $Pd_{2.8}Co@APTES\text{-}Ti_3C_2T_x$ (b), $Pd_{1.5}Fe@Ti_3C_2T_x$ (c), and $Pd_{1.7}Fe@APTES\text{-}Ti_3C_2T_x$ (d).

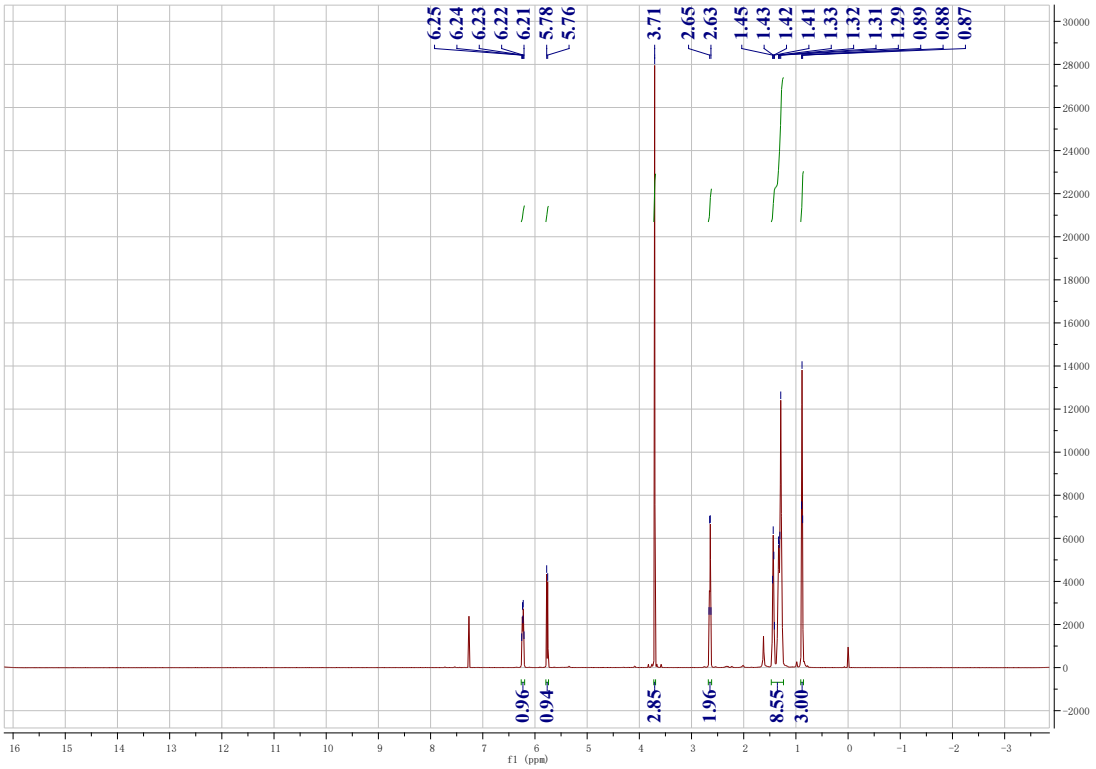

Fig S12. ^{1}H NMR spectra for (Z)-methyl non-2-enoate. ^{1}H NMR (600 MHz, $CDCl_3$): 0.88 (t, 3H, J=6 Hz), 1.29-1.45 (m, 8H), 2.63-2.65 (m, 2H), 3.71 (s, 3H), 5.77 (d, 1H, J= 12 Hz), 6.21-6.25 (dt, 1H, J=12, 6 Hz) ppm.

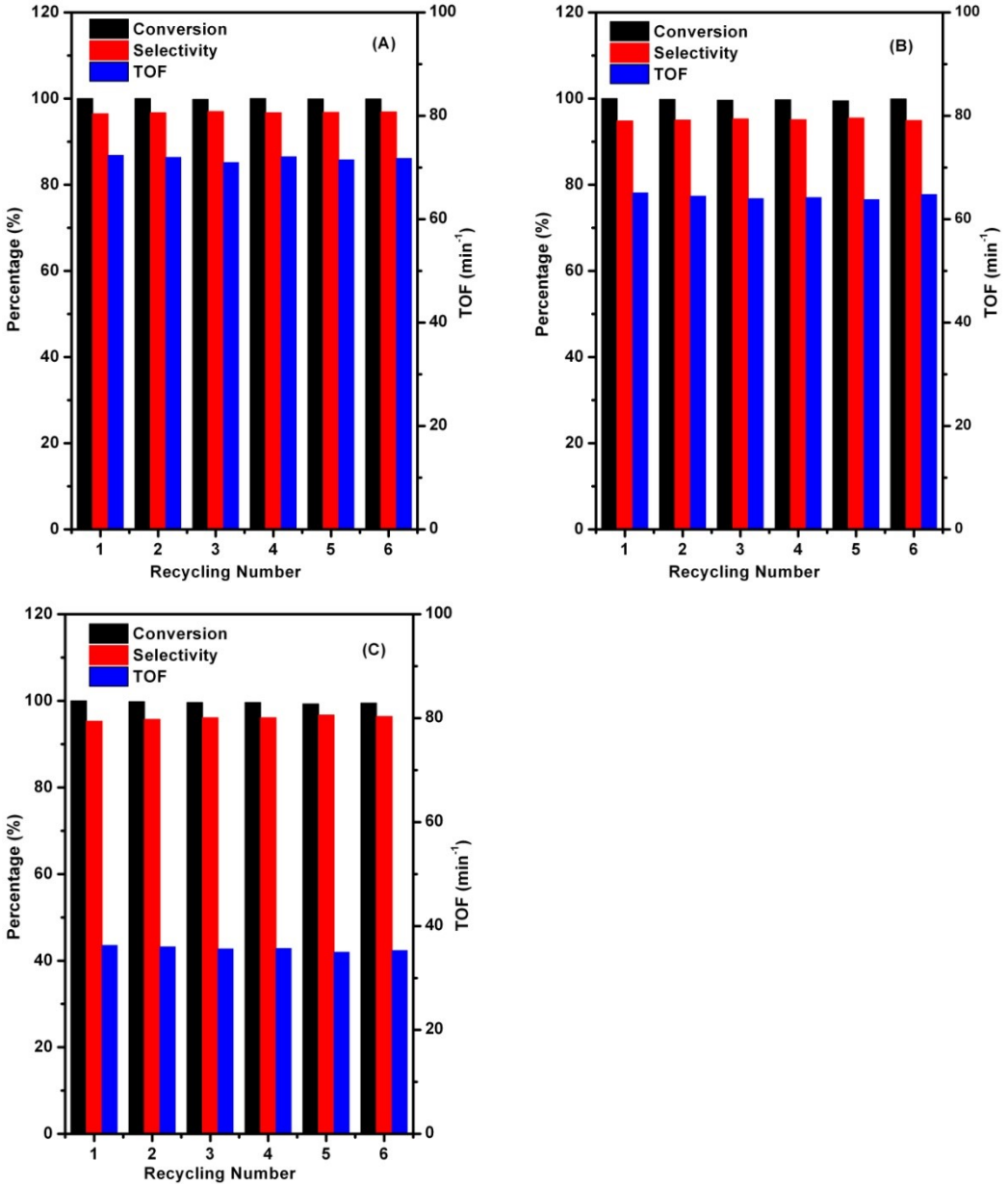

Fig S13. Conversion (black), selectivity (red), and TOF (blue) for six runs of $Pd_{1.8}Ni@Ti_3C_2T_x$ (A), $Pd_{2.6}Co@Ti_3C_2T_x$ (B), and $Pd_{1.5}Fe@Ti_3C_2T_x$ (C) in the semihydrogenation of phenylacetylene.

Table S1. Metal content and molar ratio of Pd to M (M=Fe, Co, and Ni) atoms in Pd-M@$Ti_3C_2T_x$ and Pd-M@APTES-$Ti_3C_2T_x$ catalysts.

Catalyst a	Pd (wt%)	Ni (wt%)	Co (wt%)	Fe (wt%)	n_{Pd}/n_M
Pd@$Ti_3C_2T_x$	13.31	-	-	-	1.00
$Pd_{1.8}$Ni@$Ti_3C_2T_x$	13.10	4.48	-	-	1.78
$Pd_{1.9}$Ni@APTES-$Ti_3C_2T_x$	13.49	4.43	-	-	1.86
$Pd_{2.6}$Co@$Ti_3C_2T_x$	15.21	-	3.64	-	2.63
$Pd_{2.8}$Co@APTES-$Ti_3C_2T_x$	15.55	-	3.54	-	2.77
$Pd_{1.5}$Fe@$Ti_3C_2T_x$	14.65	-	-	5.84	1.45
$Pd_{1.7}$Fe@APTES-$Ti_3C_2T_x$	16.14	-	-	5.50	1.74

a 3.0627 mg catalyst was used to analyze by ICP-MAS.

Table S2. Element content in Pd-M@$Ti_3C_2T_x$ and Pd-M@APTES-$Ti_3C_2T_x$ catalysts measured from XPS analysis.

Catalyst	Pd (at.%)	Ni/Co/Fe (at.%)	Ti (at.%)	C (at.%)	Cl (at.%)	F (at.%)	O (at.%)	N (at.%)	Si (at.%)
Pd@$Ti_3C_2T_x$	0.4	-	21.8	38.8	2.1	7.1	26.9	-	-
Pd^H@$Ti_3C_2T_x$	0.6	-	20.5	34.2	2.6	6.0	31.7	-	-
$Pd_{1.8}$Ni@$Ti_3C_2T_x$	0.3	2.1	20.6	36.6	2.3	6.8	31.3	-	-
$Pd^H_{1.8}$Ni@$Ti_3C_2T_x$	0.7	2.7	19.5	34.4	2.8	8.1	28.1	-	-
$Pd_{1.9}$Ni@APTES-$Ti_3C_2T_x$	0.3	3.1	17.1	32.3	2.1	5.2	27.6	3.5	5.1
$Pd^H_{1.9}$Ni@APTES-$Ti_3C_2T_x$	0.6	2.2	17.2	29.9	2.1	5.2	30.8	2.8	3.0
$Pd_{2.6}$Co@$Ti_3C_2T_x$	0.4	3.1	17.4	39.1	1.8	6.8	27.5	-	-
$Pd_{2.8}$Co@APTES-$Ti_3C_2T_x$	0.3	2	14.2	30.8	1.9	5.6	33.9	3.1	4.8
$Pd_{1.5}$Fe@$Ti_3C_2T_x$	0.2	1.4	16.8	29.1	1.8	4.6	33.0	-	-
$Pd_{1.7}$Fe@APTES-$Ti_3C_2T_x$	0.2	1.5	18.4	33.9	1.5	9.3	26.0	2.8	4.2

Table S3. Using Catalytic performances of Pd-M@$Ti_3C_2T_x$ (M=Fe, Co, Ni) in the semihydrogenation of methyl non-2-ynoate (R_1 = C_6H_{13} and R_2 = CO_2Me) determined by GC-MS.

Catalyst	Conversion (%)	Chemselectivity (%)	TOF (min^{-1})	Stereoselectivity Z/E
$Pd_{1.8}Ni@Ti_3C_2T_x$*	100	95.5	80.3	94/7
$Pd_{2.6}Co@Ti_3C_2T_x$**	100	94.7	78.4	92/8
$Pd_{1.5}Fe@Ti_3C_2T_x$***	100	92.6	67.4	90/10

Reaction conditions: methyl non-2-ynoate of 5.44×10^{-4} mol; THF of 3 mL; H_2 of 1 atm; Temperature at 298.15K; reaction time: *6, **8, and ***12 min.